Chapter 12
Three-Dimensional Vortex Structure Identification of Fluid Coupling and Analysis of Spatial-Temporal Evolution Mechanism

Bosen Chai, Dong Yan, Jin Zhang, Wenjie Zuo, and Guangyi Wang

Abstract The interior of fluid coupling is full of turbulent and multi-scale vortex flow. The generation, development and interaction of the multi-scale vortex structure dominate the overall internal flow. Accurate identification of unsteady multi-scale vortex structure characteristics is extremely important for revealing the law of flow and the mechanism of energy conversion and loss mechanism. The flow field of fluid coupling under braking condition is numerically simulated based on the advanced turbulence model. The temporal and spatial evolution characteristics of the three-dimensional vortex structure inside the pump wheel and turbine are extracted based on different vortex recognition methods, and the results are compared with the flow field visualization test. The accuracy and applicability of the extraction results for different vortex recognition methods are analyzed. The results show that: the threshold selection of Q method extraction vortex structure is blind. It is difficult to capture both strong and weak vortices at the same time. Ω method can accurately capture the weak vortex structure within a large threshold range. Ω-Liutex method is not sensitive to threshold selection, and it is the most effective in extracting vortex structure. From the perspective of the temporal and spatial evolution of the three-dimensional vortex structure, Ω-Liutex method can reveal the mechanism of energy conversion and loss best.

B. Chai (✉) · D. Yan · J. Zhang · W. Zuo · G. Wang
School of Mechanical and Aerospace Engineering, Jilin University, Changchun, Jilin 130025, China
e-mail: chaibs2012@jlu.edu.cn

B. Chai · W. Zuo
State Key Laboratory of Automotive Simulation and Control, Jilin University, Changchun, Jilin 130025, China

B. Chai
Sinotest Equipment Co., Ltd., Changchun, Jilin 130103, China

Y. Wang et al. (eds.), *Liutex and Third Generation of Vortex Identification*,
Springer Proceedings in Physics 288, https://doi.org/10.1007/978-981-19-8955-1_12

12.1 Introduction

With the increasing demand for energy in society, energy conservation and energy efficiency improvement have become key areas of national concern driven by the national development strategy of "carbon peaking and carbon neutrality". As a hydraulic transmission element with excellent performance of speed regulation, energy saving and emission reduction, the fluid coupling is widely used in power plants, petroleum, chemical industry, metallurgy, mining and other high energy-consuming industries. Especially in the speed regulation drive of heavy-duty and high-power equipment, the fluid coupling not only has excellent transmission performance, but also has significant energy-saving benefits [1]. The structure of the fluid coupling includes: pump wheel, turbine, and pump wheel housing, as shown in Fig. 12.1a. The pump impeller and turbine form a closed working chamber. The pump wheel rotates under the drive of the prime mover. Under the dual action of centrifugal force and blade push, The flowing medium from the pump impinges the turbine blades. The flow medium from the pump impinges the turbine blades to drive the turbine to rotate, and the energy transfer and conversion is realized in this process, as shown in Fig. 12.1b.

The working performance of the fluid coupling is determined by its internal flow characteristics. When it works, it is full of turbulent vortex flow at different scales. The generation, development and interaction of unsteady multiscale vortices govern the overall flow inside the fluid coupling, and affect its external performance. At present, there are still many key scientific problems in the accurate prediction method of the interaction relationship between the vortex flow in the fluid coupling and the flow performance. Accurately identifying the multi-scale vortex structure features inside the fluid coupling has important scientific significance for analyzing the evolution law of the internal flow field.

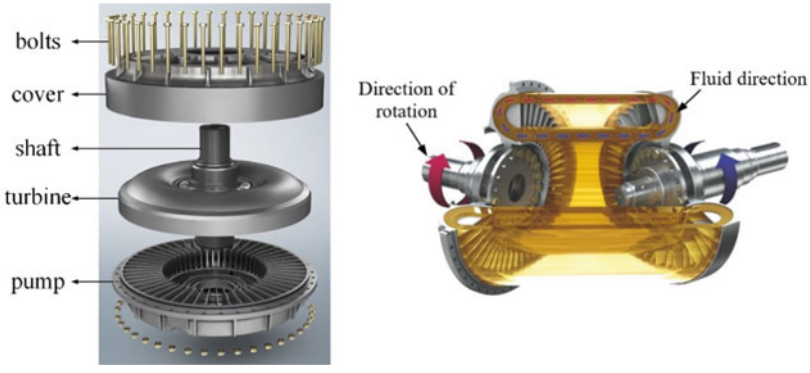

(a) Fluid coupling structure (b) Fluid flow state in the channel

Fig. 12.1 Introduction of fluid coupling

In recent years, scholars at home and abroad have carried out a lot of work in the field of vortex identification methods. They proposed a series of vortex structure identification methods and judgment criteria [2, 3]. Among them, the Q criterion is widely used [4]. However, the accuracy of the vortex structure extracted by the Q criterion depends heavily on the threshold. The physical expression of the vortex structure of this method has ambiguous meaning. In order to solve this problem, since 2014, the team of Professor Chaoqun Liu from the University of Texas at Arlington has carried out a series of research. Subsequently, a dimensionless and regularized Ω criterion and Liutex vortex vector method are proposed to accurately identify the vortex structure in the boundary layer transition flow [5, 6]. Vishwa [7] successfully applied the Liutex vortex vector method to the identification of complex vortex structures in supersonic boundary layer separation flows, which promoted the study of vortex motion and low-frequency shock wave oscillations. Charkrit [8] used Liutex method to accurately identify the hairpin vortex structure in natural flow, and the effect is more obvious. Wang [9] comprehensively applied vortex identification methods such as the Ω criterion and the Q criterion. It was found that the Burgers vortex and Sullivan vortex Ω criterion had better identification results. Guinan [10] analyzed the results of vortex motion in a visualized rotating jet based on direct numerical simulation and different vortex identification criteria. It was found that the Ω criterion and the Liutex method can identify additional small-scale vortices, while other criteria are difficult to achieve. Sun [11] used Liutex method to explore the flow characteristics in the draft tube of the turbine.

Although the third-generation vortex identification method with the Ω criterion and Liutex vortex vector method as the core has been applied in boundary layer flow and some fluid machinery fields. This is the first scientific application of the identification and extraction of unsteady multi-scale vortex structure features in the fluid coupling. In this paper, different vortex identification methods are used to extract the multi-scale vortex structure inside the hydraulic coupling based on the interactive research method of high-precision numerical simulation and flow visualization test measurement. From the perspective of the analysis of the spatiotemporal evolution mechanism of the flow field and the accurate identification of the vortex structure characteristics, the accuracy and reliability of different vortex identification aspects are evaluated. This paper highlights the practical effect of the newly developed Ω method and Ω-liutex method on the accurate identification of the internal vortex structure characteristics of the hydraulic coupling.

12.2 Simulation Model

12.2.1 Calculation Model

The effective circulation circle diameter of the square cavity fluid coupling model is 230 mm, and the blade thickness is 4 mm. Among them, the number of impeller

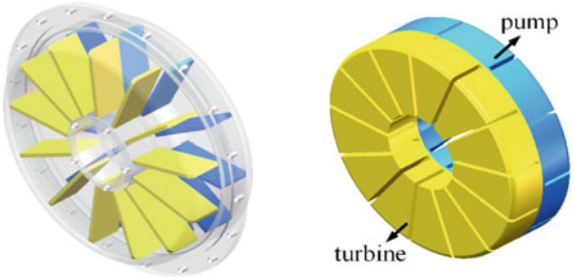

(a) 3D model (b) flow channel model

Fig. 12.2 Simulation model

(a) Overall grid (b) Turbine grid (c) Pump grid

Fig. 12.3 Grid model

blades is 13, and the number of turbine blades is 12, as shown in Fig. 12.2a. The runner model is extracted as the computational domain, as shown in Fig. 12.2b. Based on ICEM software, the hexahedral structured mesh is used to mesh the flow channel model. The number of meshes in the pump wheel flow channel is 579956, and the number of turbine flow channel meshes is 545688, with a total of 1,125,644 meshes, as shown in Fig. 12.3.

12.2.2 Turbulence Model

Based on the Large Eddy Simulation (LES) turbulence model, the improved algebraic wall model (WMLES S-Ω) is used for numerical simulation. Filtering the N-S equation, the governing equation is obtained:

$$\frac{\partial}{\partial t}(\rho\overline{u_i}) + \frac{\partial}{\partial x_j}\left(\rho\overline{u_i u_j}\right) = -\frac{\partial \overline{p_t}}{\partial x_i} + \frac{\partial}{\partial x_j}\left(\mu\frac{\partial \overline{u_i}}{\partial x_j}\right) + \frac{\partial \tau_{ij}}{\partial x_j} \tag{12.1}$$

$$\frac{\partial \overline{u_i}}{\partial x_i} = 0 \tag{12.2}$$

$$\tau_{ij} = \rho \overline{u_i u_j} - \rho \overline{u_i u_j} \tag{12.3}$$

where the sub-grid stress term τ_{ij} represents the momentum conversion between the solvable large-scale vortices and the unsolvable small-scale vortices. The WMLES S-Ω uses the large eddy simulation method outside the near-wall region, and the turbulent eddy viscosity is:

$$\mu_t = \min\left[(\kappa d_\omega)^2, \left(C_{\text{Smag}}\Delta\right)^2\right] \cdot |\text{S} - \Omega| \cdot \left\{1 - \text{e}^{-\left(y^+/25\right)^3}\right\} \tag{12.4}$$

$$\Delta = \min(\max(C_\omega \cdot d_\omega, C_\omega \cdot h_{\max}, h_{\omega n}), h_{\max}) \tag{12.5}$$

where d_ω represents the distance between the calculated point and the wall; S represents the strain rate, the Ω represents the vortex intensity, constant $\kappa = 0.41$, $C_{\text{Smag}} = 0.2$, $C_\omega = 0.15$. Filter size Δ is selected according to flow field conditions, $h_{\max}$ represents the maximum side length of the hexahedral element, $h_{\omega n}$ represents the grid spacing in the normal direction of the wall.

12.2.3 Simulation Parameters

Table 12.1 shows the basic parameters of fluid coupling under braking condition. Pure water is used as the flow medium of this model. Due to the slow speed, the influence of temperature rise and leakage is ignored. The flow field structure distribution in the mainstream area of the flow channel is complex. The large eddy simulation turbulence model is selected for simulation analysis [12].

Table 12.1 Parameter setting

Parameter type	Parameters
Time step	0.01 s
Iteration steps	300
Convergent residual	10^{-4}
Medium viscosity	0.001003 Pa·s
Algorithm selection	SIMPLE algorithm
Boundary conditions	Smooth wall without slippage

12.3 Eddy Identification Criterion

12.3.1 Q Criterion

Hunt [13] proposed to use the second Galilean invariant of the velocity gradient tensor to represent the vortex structure. The velocity gradient tensor is decomposed into a symmetric part and an anti-symmetric part. Through the Cauchy-Stokes decomposition, the Q expression can be written as:

$$Q = \frac{1}{2}\left(\|B\|_{\mathrm{F}}^2 - \|A\|_{\mathrm{F}}^2\right) \tag{12.6}$$

where $\|\|_{\mathrm{F}}^2$ is the Frobenius norm of the matrix. The physical significance of Q lies in the fact that not only the vorticity is required in the vortex structure, but also the anti-symmetric tensor B needs to be able to overcome the deformation effect represented by the symmetric tensor A. In practical applications, the threshold $Q_{threshold}$ must be used to determine the vortex area, and $Q > Q_{threshold}$ is defined as the vortex.

12.3.2 Omega Vortex Identification Method

Since the vortex is an area where the vorticity exceeds the deformation, and the vorticity cannot directly represent the fluid rotation. Therefore, the ratio of vorticity to deformation is considered to facilitate the identification of vortices.Vorticity $\boldsymbol{\omega}$ cannot represent the rotational movement of the fluid, The $\boldsymbol{\omega}$ is decomposed into a rotating part and a non-rotating part:

$$\boldsymbol{\omega} = \boldsymbol{R} + \boldsymbol{S} \tag{12.7}$$

where $\boldsymbol{R}$ is the vorticity of the rotating part, $\boldsymbol{S}$ is the non-rotating part vorticity. Generally speaking, the directions of $\boldsymbol{R}$ and $\boldsymbol{\omega}$ are different. The parameter Ω is quoted to represent the ratio of the vorticity of the rotating part to the total vorticity. The Ω can be presented as:

$$\Omega = \frac{\|B\|_F^2}{\|A\|_F^2 + \|B\|_F^2} \tag{12.8}$$

In order to prevent the problem of division by zero, a small positive number is added to the denominator term of formula (12.8). The Ω expression becomes

$$\Omega = \frac{\|B\|_F^2}{\|A\|_F^2 + \|B\|_F^2 + \varepsilon} \tag{12.9}$$

where the value range of Ω is reduced to $0 \leq \Omega \leq 1$, which represents the concentration of vorticity. When the $\Omega = 1$, it means that the fluid does a rigid body rotation.

12.3.3 Omega-Liutex Vortex Identification Method

Proposal based on Ω method and Liutex vector, scholars [14] combined the two to propose the Ω-Liutex vortex recognition method. Denoted as Ω_L method. The Ω_L is defined as:

$$\mathbf{\Omega}_L = \frac{\beta^2}{\alpha^2 + \beta^2 + \varepsilon} \tag{12.10}$$

Introduce small positive number ε into the denominator of Ω_L to eliminate non-physical noise, ε is defined by experience as

$$\varepsilon = b \times \left(\beta^2 - \alpha^2\right)_{\max} \tag{12.11}$$

where b is a small positive number, e.g., 0.001. For each case, b is a fixed parameter and the term $\left(\beta^2 - \alpha^2\right)_{\max}$ can be easily obtained at each time step and the manual adjustment of ε is avoided. The α and β are the two-dimensional principal strain rate and vorticity on a plane perpendicular to the local axis of rotation, respectively.

12.4 Vortex Recognition Image and Analysis

12.4.1 Analysis of Threshold Selection Range

Different vortex identification criteria are used for the threshold selection range of the three-dimensional vortex structure extraction inside the fluid coupling channel. The threshold ranges of the Ω method and the Ω-Liutex method are normalized. In order to facilitate the comparison of the threshold range, the threshold range extracted by the Q criterion is proportionally reduced to 0~1, which are listed in Table 12.2.

Table 12.2 Threshold selection range under different vortex identification criteria

Vortex identification criterion	Minimum threshold	Maximum threshold	Optimal threshold
Q Criterion	0	1	0.18
Ω	0	0.992187	0.56
Ω-Liutex	0	0.997305	0.52

The Q criterion is selected to extract the three-dimensional vortex structure of the flow channel. When the threshold value is higher than 0.3, the three-dimensional vortex structure inside the flow channel is obviously broken. And there are weak vortex structures in the flow channel. The three-dimensional vortex structure is complete, but the extracted vortex structures are mixed when the threshold value is too small. The $Q = 0.18$ is finally determined as the optimal threshold after repeated extraction.

The threshold range of the Ω method is selected from 0 to 0.992187. Although the three-dimensional vortex extracted by the recommended threshold [15] of 0.52 is complete. The vortex structure near the wall has the phenomenon of mutual adhesion. When the threshold is gradually increased from 0.52 to 0.6, the overall variation of the three-dimensional vortex in the flow channel is small, and the adhesion between vortex structures of different scales is reduced. After many attempts, the optimal threshold of this method is determined to be 0.56. The threshold range of the Ω-Liutex method is selected from 0 to 0.997305, which is similar to the threshold range of the Ω method. And when the threshold is reduced to between 0.52 and 0.6, the extracted vortex structure changes little. At this time, the three-dimensional vortex structure in the flow channel can not only reflect the overall motion state of the fluid, but also the main vortex structure is divided into clearly visible multi-scale vortex structures.

To sum up, the threshold range can be reduced to 0~0.3 when the Q criterion is used, but the change of the threshold seriously affects the extraction effect of the vortex structure. When the Ω method and the Ω-Liutex method are used, the threshold range is reduced to 0.52~0.6. The extracted vortex structure is clear and accurate, and is less affected by the threshold.

12.4.2 Three-Dimensional Vortex Structure Analysis

Under the braking condition, the internal circulation phenomenon of the turbine flow channel is extremely obvious, the turbulent flow structure is complex, and the three-dimensional vortex structure information is rich, which is shown in Fig. 12.4. In the mainstream area of the turbine, a large-scale vortex-like strong vortex structure is formed, and a small-scale vortex-like weak vortex structure is formed near the blade wall and the outer ring.

Longitudinally, different vortex identification criteria are used to extract the vortex structure of the turbine runner, as shown in Fig. 12.5. Based on the Q criterion, the threshold value $Q = 0.18$ is selected to extract the vortex structure inside the turbine flow channel. As shown in Fig. 12.5a, the large-scale vortex are distributed in the mainstream area, and close to the blades and near the wall surface. The extraction effect of small-scale vortex is obvious.

Based on the Ω method, the recommended threshold $\Omega = 0.52$ is used to extract the vortex structure [15]. As shown in Fig. 12.5a and b, while the Ω method captures the strong vortex structure, the recognition effect of the weak vortex structure near

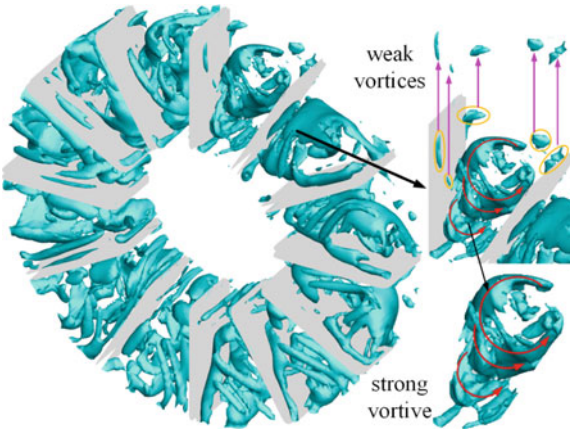

Fig. 12.4 Distribution of multi-scale vortex structure in fluid coupling channel

the wall area is clear, and it can reflect the overall large vortex flow trend in the flow channel. However, most of the strong vortex structures extracted from the mainstream area are strong vortex structures, and there are few weak vortex structures.

On this basis, combined with the advantages of the Liutex method, $\Omega_L = 0.52$ is selected to extract the three-dimensional vortex structure, as shown in Fig. 12.5c. This method has the best effect on feature extraction of 3D vortex structures. And it can capture both strong and weak vortex structures in the flow channel. In particular, the vortex structure extraction in the near-wall area and the runner corner area is more abundant. It can highlight the multi-layered sense of the multi-scale vortex structure inside the flow channel, and present the dynamic evolution process of the stretching, twisting and tearing of the vortex structure at different scales.

Horizontally, the thresholds of the Q criterion are selected as 0.18, 0.22 and 0.26 in Fig. 12.5a. The small-scale adjustment of the threshold has obvious differences in the effect of vortex structure extraction. Although the vortex structure characteristics inside the turbine channel can be displayed under the appropriate threshold selection, the vortex identification method based on the Q criterion is extremely sensitive to the threshold selection. The application of this method is limited by the precise selection of the threshold, and the blind selection is often large, and the efficiency of accurately identifying the vortex structure features is low.

In order to facilitate comparative analysis, in the form of arithmetic progression, the threshold size in the Ω and Ω_L methods is increased. In the Ω method, as the threshold increases, the elongated vortex structure near the wall is fractured. The block vortex structure gradually decreases, the change of the strong vortex structure inside the flow channel is small, and the sensitivity to the threshold decreases, as shown in Fig. 12.5b. In the Ω_L method, as the threshold increases, the vortex structure extraction effect has little effect. Only a small number of small-scale vortex structures change slightly, and the overall change trend is least affected by the threshold. The Ω-Liutex method measures the relative strength of the fluid. In the complex flow field structure, the distribution of strong and weak vortex is different, and it is difficult

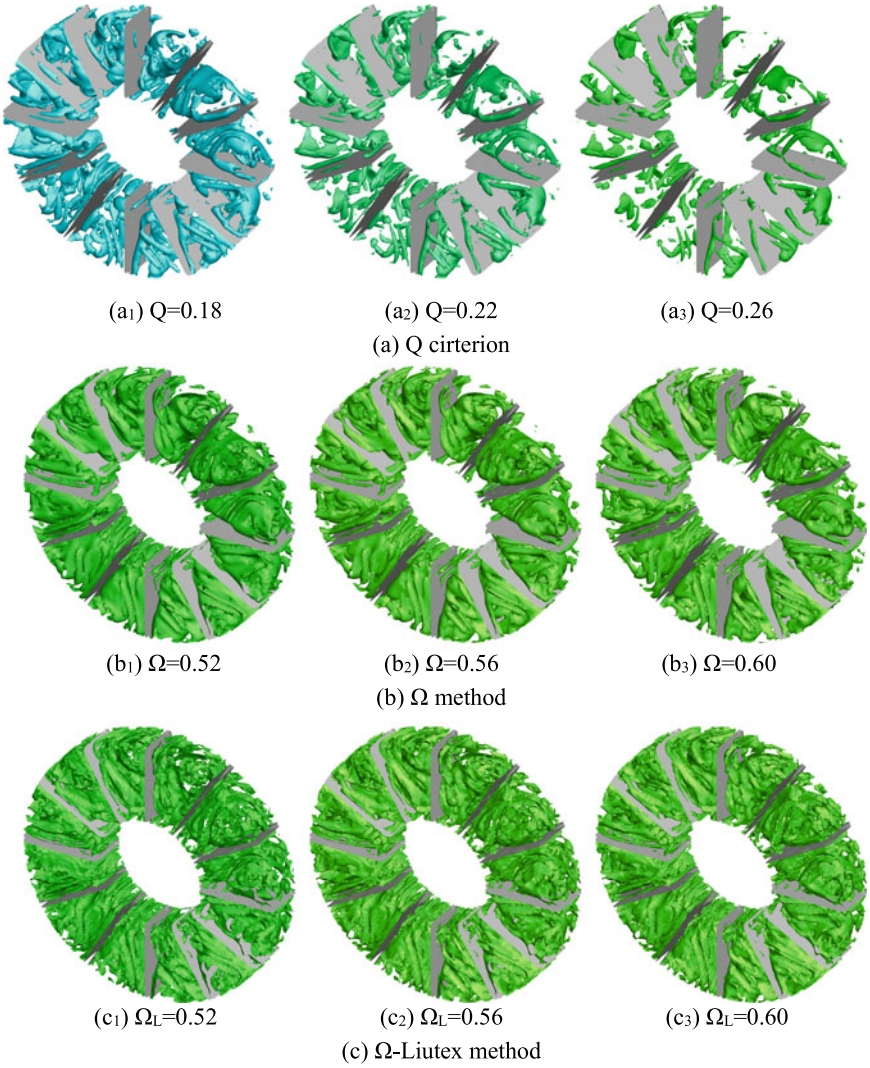

Fig. 12.5 Multi-scale vortex structure inside the flow channel under different thresholds

to select an appropriate threshold in all fluid structures by absolute strength. The relative intensity dynamically adjusts the threshold range based on the distribution of the vortex structure in the flow field itself, and the effect of the threshold selection on the vortex structure is reduced. Therefore, the Ω-Liutex method is selected to extract the vortex structure inside the fluid coupling channel with the best effect and the highest efficiency.

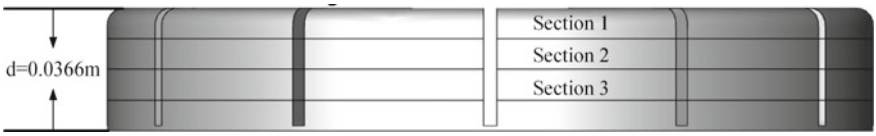

Fig. 12.6 Turbine flow channel isometric diagram

12.4.3 Two-Dimensional Vortex Flow Field Analysis

In order to facilitate the comparison and analysis of the theoretical and two-dimensional flow field visualization test results and compare the ability of different vortex identification methods to accurately capture the vortex structure inside the fluid coupling channel. Three sections of the turbine flow channel are taken along the radial direction, namely the upper section 1, the middle section 2 and the lower section 3, as shown in Fig. 12.6. The distances of each section from the outer wall of the turbine are: section 1 = 9.15 mm, section 2 = 18.3 mm, and section 3 = 27.45 mm. The vorticity information extracted from each section using different vortex identification methods is shown in Fig. 12.7.

12.4.4 Text Verification

Based on the laser section flow field visualization test platform, the flow field image was collected by Particle Image Velocimetry (PIV), as shown in Fig. 12.8. The internal flow medium of the transparent fluid coupling test prototype is pure water. Under the state of full liquid filling, PSP tracer particles with a diameter of 1.5 μm are evenly injected into the test prototype. The continuous laser outputs fan-shaped laser light. The flow field inside the turbine is illuminated [16]. Three groups of flow field visualization experiments were carried out for the turbine flow channel. Adjust the spatial position of the laser sheet light. In the three groups of experiments, the laser sheet light is adjusted to coincide with the upper section 1, the middle section 2 and the lower section 3 respectively. Due to space limitations, this paper only takes the middle section as an example to collect flow field visualization images and post-process the experimental data.

Under braking condition, the pump wheel speed is adjusted to 300r/min, and the turbine speed is 0r/min. Adjust the laser sheet light to coincide with the middle section of the turbine runner. The optical axis of the CCD camera is perpendicular to the outer wall of the turbine of the sample prototype, and two consecutive frames of flow images are collected, as shown in Fig. 12.9a. Based on the PIVlab program [17], the normalized cross-correlation algorithm is used to calculate two consecutive images, and the flow field vorticity information is extracted, as shown in Fig. 12.9b.

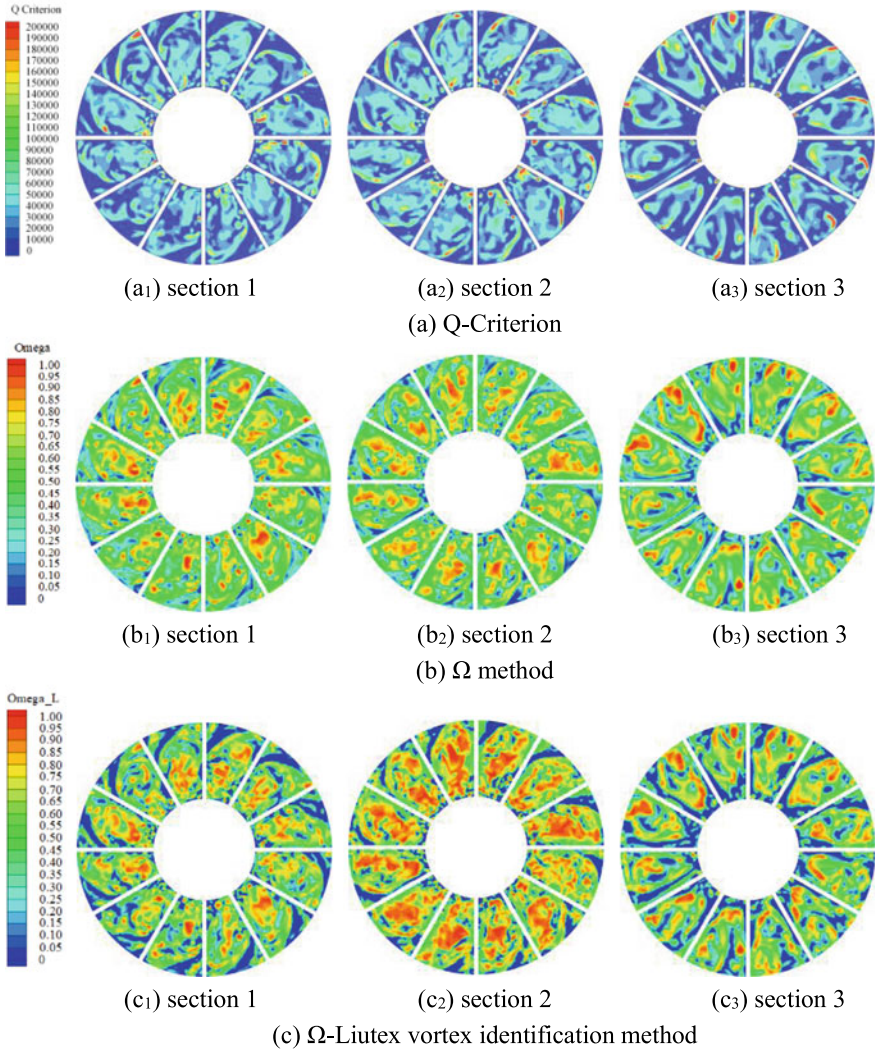

(a_1) section 1 (a_2) section 2 (a_3) section 3

(a) Q-Criterion

(b_1) section 1 (b_2) section 2 (b_3) section 3

(b) Ω method

(c_1) section 1 (c_2) section 2 (c_3) section 3

(c) Ω-Liutex vortex identification method

Fig. 12.7 Cross-section view of vorticity in turbine runner

12.5 Analysis and Discussion

12.5.1 Two-Dimensional Cross-Sectional Flow Field

For Sect. 12.2, the small-scale vortex structure cannot be accurately captured by the outer ring region extracted using the Q criterion. The three-dimensional vortex structure of different scales near the inner ring is doped, and the extraction effect

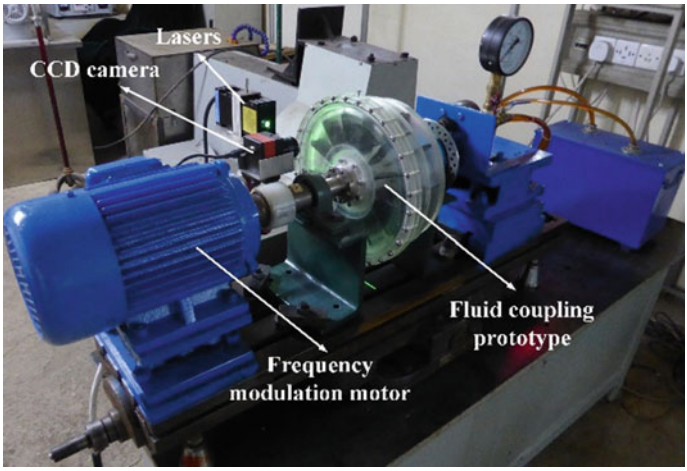

Fig. 12.8 Laser section flow field visualization test platform

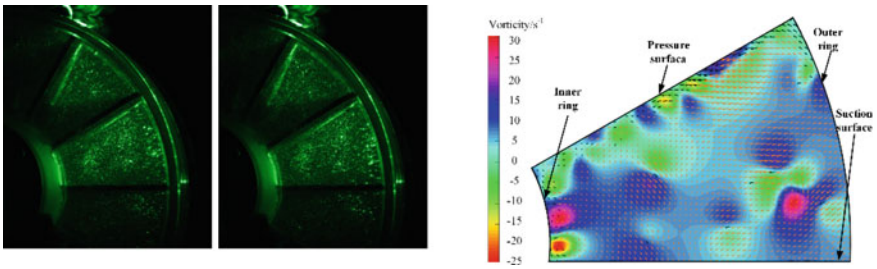

(a) image acquisition (b) image post-processing

Fig. 12.9 Experimental image processing

is blurred, which is difficult to assist the analysis of the test results. When the Ω method is adopted, the high-speed fluid in the pump wheel with the tendency of circular motion flows into the turbine flow channel. At this time, the multi-scale vortex are accelerated and flow into the inside of the flow channel under the action of "lifting and throwing" of the circular arc surface of the outer ring. At the same time, the flow channel changes from wide to narrow. Under the combined action of the two, the fluid accumulates to form a large-scale vortex. The vortex structure near the inner ring is complex, and small-scale vortex can be clearly captured. When the Ω-Liutex method is used, the flow trend of the incident fluid in the flow channel after entering the flow channel can be analyzed through the distribution of the three-dimensional vortex structure in the weak vortex region. The three-dimensional vortex structure in the main flow area completely depicts the diversion of the fluid after impingement through the blades.

For Sect. 12.3, using the Q criterion to extract the three dimensional vortex structure is too dependent on the choice of threshold. While extracting the strong vortex structure in the mainstream area, the capture effect of the weak vortex structure is poor. It is difficult to select an appropriate threshold range to completely capture its overall vortex structure characteristics. When the Ω method is used, the shape of the fluid vortex structure extracted in the mainstream region is large. The fluid velocity near the pressure surface vane is fast, the flow channel begins to fill with liquid, the vortex structure becomes smaller, and the large vortex structure in the flow channel gradually forms. When the Ω-Liutex method is used, large-scale vortex are formed by the accumulation of slow fluid in the middle region of the flow channel. The high-speed fluid at the inlet rotates and rises, and the fluid velocity at the center of the flow channel after the flow channel is filled with liquid drops through the impact of the vane and the wall surface. The high-speed fluid near the upper end of the inner ring merges with the slow flow at the intermediate interface to form a small-scale vortex.

For Sect. 12.4, when the Q criterion is used, the small-scale vortex structure can be accurately captured near the inner ring of the flow channel. However, the overall vortex structure distribution gradient is poor, and the effect is blurred. When the Ω method is used, the fluid near the section flows out from the turbine outlet. The fluid velocity increases, and the scale vortex structure formed after the high-speed flow hits the blades near the inner ring gradually decreases.

The vortex structure extracted by the Ω-Liutex method not only has the advantages of the Ω method, but also the layering effect of the vortex structure is more obvious. It can separate the discontinuous structure in the shear layer from the rotating vortex, and the overall trend of the captured vortex structure is better than the Ω method.

12.5.2 Visual Analysis of Flow Field in Vortex Structure

The numerical simulation results of the single flow channel of the fluid coupling extracted by the Ω-Liutex method are compared with the vortex structure extracted from the flow field visualization test, as shown in Fig. 12.10. For the convenience of analysis, the runner area is divided into six main areas, labeled 1~6 respectively. Among them, regions 1 and 2 are close to the outlet of the flow channel, regions 3 and 4 are close to the pressure surface of the flow channel, region 5 is close to the inlet of the flow channel, and region 6 is close to the suction surface of the flow channel.

Regions 1 and 2 near the inner ring of the runner are the outlet of the runner. The high-speed fluid inside the flow channel is returned to the vicinity of the outlet by the impact of the pressure surface. Part of the fluid flows out of the outlet which causes the flow rate to slow down. Close to the inner ring space of the flow channel, the space becomes narrow, and the fluid accumulates into a strong vortex structure here. The high-speed flow from the pump wheel is continuously poured in from the inlet. The fluid inside the turbine rotates around the central area, forming a large-scale

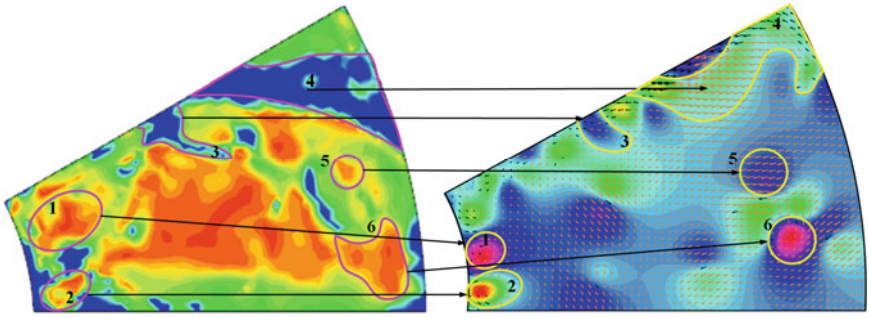

(a) Numerical simulation results (b) PIV processing results

Fig. 12.10 Results comparison

vortex dominated by the center of the flow channel. At this time, the fluid that has not yet impacted the pressure surface has a circular motion tendency, and the flow speed is fast, forming a large-area weak vortex structure in regions 3 and 4. As the fluid flows in the flow channel, the high-speed fluid from areas 3 and 4 pushes the low-speed flow in areas 1 and 2, and pushes the fluid to transfer energy in the flow channel. At this time, part of the slow-moving fluid gradually forms a swirl near the wall of the flow channel, the fluid velocity slows down, and a strong vortex structure is formed in this area.

12.6 Conclusions

The multi-scale vortex structure inside the fluid coupling is extracted by different vortex identification methods. Based on the threshold selection dependence and the vortex structure extraction effect, the applicability of different vortex identification methods is compared in detail.

(1) In terms of threshold selection. The Q criterion takes the absolute strength of the fluid as the threshold. The threshold selection range of vortex structure extraction is large. It is necessary to continuously adjust and determine the appropriate threshold selection range, which leads to the blindness of threshold selection and low vortex extraction efficiency. The Ω method and the Ω-Liutex method use the relative strength of the fluid as the threshold, which effectively reduces the workload of threshold selection and improves the efficiency of vortex extraction. The threshold range is narrowed to 0.52–0.6, which can effectively improve the vortex structure extraction effect, and has little dependence on the threshold selection.

(2) In terms of the effect of vortex structure extraction, The Q criterion can only extract vortex structures with small intensity differences in the flow field. And it is difficult to capture both strong and weak vortex at the same time. The Ω

method can accurately display the strong vortex structure, and the extraction effect of the weak vortex structure is also significantly improved. The Ω-Liutex method improves the distribution effect of the Ω method to extract the overall vortex structure. While capturing strong and weak vortex, it can clearly reflect the trend of fluid flow in the flow channel. The ability of this method to capture the vortex structure of the fluid coupling is obviously better than that of the Q criterion and the Ω method.

Funding The authors disclosed receipt of the following financial support for the research, authorship, and/or publication of this article: This work was supported by the National Natural Science Foundation of China (grant no.52075212, 51405184), Scientific research project of Jilin Provincial Department of Education (grant no. JJKH20220977KJ), Free Exploration Project of the State Key Laboratory of Automotive Simulation and Control, Jilin University (grant no. ascl-zytsxm-202010), Funded by the special fund for the basic scientific research business expenses of the central colleges and universities of Chang'an University(grant no. 300102251511), and General Program of China Postdoctoral Science Foundation (grant no. 2018M641776).

References

1. C. Chu, W. Ma, *Construction Machinery Hydraulic and Hydraulic Transmission System (Hydraulic volume)* (Chemical Industry Press, Beijing, 2015)
2. Y. Zhang, X. Qiu, F. Chen et al., A selected review of vortex identification methods with applications. J. Hydrodyn. **30**(5), 767–779 (2018)
3. B. Epps, *Review of Vortex Identification Methods*. Aiaa Aerospace Sciences Meeting (2017)
4. Y. Wang, N. Gui, A review of the third-generation vortex identification method and its applications. Chin. J. Hydrodyn. **34**(4), 413–429 (2019)
5. C. Liu, Y. Wang, Y. Yang et al., New omega vortex identification method. Mech. Astron. **59**(8), 62–70 (2016)
6. C. Liu, Y. Gao, S. Tian et al., Rortex—a new vortex vector definition and vorticity tensor and vector decompositions. Phys. Fluids **30**(3), 035103 (2018)
7. V. Patel, Y. Yan, Y. Yu, et al., Correlation analysis between low-frequency shock oscillation and Liutex in SBLI, in *Liutex and Third Generation of Vortex Definition and Identification* (2021), pp. 263–277
8. S. Charkri, P. Shrestha, C. Liu, Liutex core line and POD analysis on hairpin vortex formation in natural flow transition. J. Hydrodyn. **32**(6), 1109–1121 (2020)
9. Y. Wang, S. Fu, On the thresholds of vortex identification methods, in *Fluid Structure Sound Interactions and Control* (2019), pp. 45–49
10. N. Gui, L. Ge, P. Cheng et al., Comparative assessment and analysis of rorticity by Rortex in swirling jets. J. Hydrodyn. **31**, 495–503 (2019)
11. L. Sun, P. Guo, X. Luo, Visualization investigation into precessing vortex rope in Francis turbine draft tube based on several vortex identification criterions. Chin. J. Hydrodyn. **34**(06), 779–787 (2019)
12. B. Chai, Y. Xiang, W. Ma et al., Analysis and experimental verification of turbulence models in flow simulation for hydrodynamic coupling under braking condition. Trans. Chin. Soc. Agric. Eng. **32**(03), 34–40 (2016)
13. C. Liu, Y. Gao, X. Dong et al., Third generation of vortex identification methods: omega and Liutex/Rortex based systems. J. Hydrodyn. **31**(2), 205–223 (2019)

14. X. Dong, Y. Gao, C. Liu, New normalized Rortex/vortex identification method. Phys. Fluids **31**(1), 011701 (2019)
15. C. Liu, Liutex-third generation of vortex definition and identification methods. Acta Aerodyn. Sin. **38**(3), 413–431 (2020)
16. B. Chai, Study on Visualization of Internal Flow in Hydrodynamic Coupling and Recognition Method of Flow Velocity (2012)
17. M. Ochowiak, S. Włodarczak, A. Krupińska, et al., Particle image velocimetry based on Matlab and PIVlab for testing flow disturbing elements. Lect. Notes Mech. Eng. **9**(1), 268–276 (2021)